

# Variational Phasor Circuits for Phase-Native Brain-Computer Interface Classification

Dibakar Sigdel<sup>1\*</sup>

<sup>1</sup> Mindverse Computing LLC, WA 98087

March 20, 2026

## Abstract

We present the **Variational Phasor Circuit (VPC)**, a deterministic classical learning architecture operating on the continuous  $S^1$  unit circle manifold. Inspired by variational quantum circuits, VPC replaces dense real-valued weight matrices with trainable phase shifts, local unitary mixing, and structured interference in the ambient complex space. This phase-native design provides a unified method for both binary and multi-class classification of spatially distributed signals. A single VPC block supports compact phase-based decision boundaries, while stacked VPC compositions extend the model to deeper circuits through inter-block pull-back normalization. Using synthetic brain-computer interface benchmarks, we show that VPC can decode difficult mental-state classification tasks with competitive accuracy and substantially fewer trainable parameters than standard Euclidean baselines. These results position unit-circle phase interference as a practical and mathematically principled alternative to dense neural computation, and motivate VPC as both a standalone classifier and a front-end encoding layer for future hybrid phasor-quantum systems.

## 1 Introduction

Electroencephalography (EEG) and brain-computer interface (BCI) research have long served as demanding benchmarks for machine learning because mental-state decoding requires the discrimination of weak, noisy, spatially correlated, and strongly non-stationary signals. The classical BCI literature has therefore explored a wide range of classifiers, from linear discriminants and support vector machines to ensemble methods and multilayer neural networks, each balancing robustness, calibration, and computational cost in different ways [6]. At the same time, the underlying neurophysics of EEG is intrinsically oscillatory: signals are generated by coupled cortical sources whose observable structure depends not only on amplitude but also on synchronization, phase relationships, and distributed field interactions across electrodes [10]. This makes BCI classification a natural setting in which to ask whether phase-native learning architectures can offer a better inductive bias than standard Euclidean feature processing.

Historically, foundational BCI systems established the communication-and-control paradigm and emphasized practical trade-offs among signal quality, model complexity, and real-time reliability [16]. More recent reviews document a methodological progression from handcrafted spectral/spatial features and shallow classifiers to increasingly deep representation-learning pipelines [6]. In parallel, the theory of coupled oscillators has provided a rigorous language for synchronization, phase-locking, and collective dynamics in complex systems [5, 15], which aligns naturally with phase-centric perspectives on neural data. These two threads—practical

---

\*devdeep137@gmail.com

BCI machine learning and phase-dynamics theory—motivate architectures that treat phase geometry as a first-class computational object rather than as a derived feature.

Most contemporary machine-learning pipelines still operate through dense real-valued parameter matrices. Whether the model is a shallow multilayer perceptron or a larger attention-based architecture, the dominant computational primitive remains the learned affine map in  $\mathbb{R}^N$ . Such models are flexible, but their parameter count and memory footprint scale rapidly with feature dimension, and they do not natively enforce the angular or interference structure that often characterizes oscillatory biosignals. In practice, this means that representations of phase-coherent EEG states are frequently mediated by over-parameterized real-valued layers whose geometry is only indirectly related to the signal domain itself.

Quantum machine learning offers an alternative viewpoint. Parameterized and variational quantum circuits replace dense Euclidean weight matrices with sequences of unitary operations acting on encoded states in Hilbert space [1, 3]. This line of work has made parameter efficiency and data encoding central design questions, since the expressive power of the model depends strongly on how classical information is loaded into phase and amplitude coordinates [13]. Yet practical deployment remains constrained by noisy intermediate-scale quantum hardware, limited qubit counts, and difficult optimization phenomena such as barren plateaus [7]. These limitations motivate a classical analogue that retains the useful unitary, phase-centric structure of variational circuits without inheriting the hardware burden of current quantum devices.

Within the VQC literature itself, multiple formulations have reinforced this perspective: circuit-centric quantum classifiers formalize model families around explicit unitary templates [12], hybrid variational theory clarifies optimization principles for parameterized quantum-classical workflows [8], and quantum circuit learning demonstrates how trainable unitary stacks can perform supervised function approximation [9]. Taken together, these results suggest that structured unitary computation is a powerful inductive bias even before fault-tolerant quantum hardware is widely available.

That analogue is provided by the broader PhasorFlow framework [14], which formalizes computation on the unit circle  $S^1$  and on the torus  $\mathbb{T}^N$  using deterministic phasor states, unitary interference operators, and explicit pull-back operations. Within that framework, the **Variational Phasor Circuit** (VPC) can be understood as a phase-native classical learning model: data are encoded as unit-magnitude complex states  $z_k = e^{i\phi_k}$ , trainable parameters enter only as phase shifts, and global structure is induced through local mixing and spectral interference rather than through dense learned Euclidean matrices. The result is a deterministic architecture whose trainable complexity scales linearly with the number of computational threads, while still supporting non-trivial interference dynamics in the ambient space  $\mathbb{C}^N$ .

This phase-native formulation is especially relevant for EEG and BCI. Because electrode snapshots can be mapped directly to bounded phase coordinates, the encoder preserves the distributed spatial organization of the measurement rather than flattening it immediately into an unconstrained real-valued feature vector. The same bounded representation also makes VPC a plausible *buffer* or interface layer for future hybrid quantum workflows: a classical phasor front-end can absorb raw BCI variability, stabilize it on  $\mathbb{T}^N$ , and pass structured phase coordinates to downstream quantum or variational quantum models when such hardware becomes practical. In that sense, VPC is not only a standalone classifier but also a candidate preprocessing and encoding system for future phasor-to-qubit pipelines, where careful classical data encoding is already known to be a decisive factor in quantum-model performance [13].

In this paper, we develop the mathematical construction of VPC and test it on a synthetic 32-channel BrainFlow-based BCI benchmark [2]. The task is designed around binary and four-class mental-state decoding, where the classes differ by distributed spatial phase structure rather than by a simple scalar threshold. Our objective is not merely to show that VPC can classify EEG-like data, but to establish why it is significant: it offers a phase-aligned, low-parameter, fully deterministic alternative to dense neural classifiers, and it provides a concrete computational

bridge between classical oscillatory signal processing and future hybrid quantum systems.

The main contributions of this manuscript are threefold:

1. We formalize the Variational Phasor Circuit as a deterministic, unit-circle learning architecture derived from the PhasorFlow framework, clarifying its relation to variational quantum circuits while remaining fully classical.
2. We position VPC in the context of BCI and EEG literature as a phase-native model for mental-state classification, motivated by the oscillatory and spatially distributed structure of neural measurements.
3. We demonstrate empirically that shallow and depth-scaled VPC models can achieve strong BCI classification performance with drastically fewer trainable parameters than standard dense baselines, while also serving as a plausible front-end encoding layer for future phasor-quantum pipelines.

## 2 Theory

This section develops VPC in four components: (i) phasor state geometry on  $\mathbb{T}^N$ , (ii) unitary gate primitives in the ambient space  $\mathbb{C}^N$ , (iii) single-block VPC operators, and (iv) deep composition with inter-block pull-back.

### 2.1 Phasor State Vectors

Unlike a classical computer which manipulates discrete binary strings  $b \in \{0, 1\}^N$ , or a quantum computer operating on complex probability amplitudes  $|\psi\rangle$ , a Phasor computer operates entirely on continuous angular states in the interval  $[-\pi, \pi]$ . Each computational thread is a unit-magnitude complex number identified with  $U(1)$ :

$$z = e^{i\phi}, \quad \phi \in [-\pi, \pi]. \quad (1)$$

For  $N$  threads, the encoded state is

$$\mathbf{z} = (e^{i\phi_1}, \dots, e^{i\phi_N})^\top \in \mathbb{T}^N \subset \mathbb{C}^N, \quad (2)$$

where  $\phi_k \in [-\pi, \pi]$  is the phase coordinate of thread  $k$ .

**Definition 2.1** (VPC State Manifold). *For  $N$  computational threads, the admissible state manifold is*

$$\mathcal{M}_{\text{VPC}} = \mathbb{T}^N = \{\mathbf{z} \in \mathbb{C}^N : |z_k| = 1, k = 1, \dots, N\}. \quad (3)$$

We reserve  $\phi$  for phasor-state angles and use  $\theta$  for trainable gate parameters.

**Definition 2.2** (Ambient Complex Extension). *Although admissible phasor states lie on  $\mathbb{T}^N$ , linear interference operators act on the ambient vector space  $\mathbb{C}^N$ . Hence a unitary map  $U \in U(N)$  preserves global  $\ell^2$  energy but need not preserve coordinatewise unit modulus.*

### 2.2 Unitary Gate Primitives

The VPC block uses two unitary operator classes:

$$S(\boldsymbol{\theta}) = \text{diag}\left(e^{i\theta_1}, \dots, e^{i\theta_N}\right) \in U(1)^N \subset U(N), \quad M_{j,k} = \frac{1}{\sqrt{2}} \begin{pmatrix} 1 & i \\ i & 1 \end{pmatrix} \in U(2). \quad (4)$$

$S(\boldsymbol{\theta})$  is a coordinatewise phase rotation that preserves  $\mathbb{T}^N$  exactly;  $M_{j,k}$  is a local beam-splitter coupling adjacent threads  $j$  and  $k$ .

Applying  $M_{j,k}$  to  $(z_j, z_k) = (e^{i\phi_j}, e^{i\phi_k})$  yields  $|z'_j|^2 = 1 + \sin(\phi_j - \phi_k)$ , so individual thread magnitudes can depart from unity while global  $\ell^2$  energy is conserved.

**Proposition 2.1** (Unitary Mixing Extends VPC States into  $\mathbb{C}^N$ ). *Let  $\mathbf{z} \in \mathbb{T}^N$  and let  $U \in U(N)$  be a non-diagonal mixing operator. Then*

$$\|U\mathbf{z}\|_2 = \|\mathbf{z}\|_2 = \sqrt{N}, \quad (5)$$

but in general  $U\mathbf{z} \notin \mathbb{T}^N$  because the coordinatewise modulus constraints  $|(U\mathbf{z})_k| = 1$  need not hold.

### 2.3 Single-Block VPC Operator

Given encoded input state  $\mathbf{z}_{\text{in}} \in \mathbb{T}^N$ , a single VPC block is

$$\mathcal{V}(\boldsymbol{\theta}) = U_{\text{local}} \left( \prod_{k=1}^N S_k(\theta_k) \right), \quad U_{\text{local}} = \prod_{k=0,2,4,\dots} M_{k,k+1}, \quad (6)$$

with forward state  $\mathbf{z}_f = \mathcal{V}(\boldsymbol{\theta})\mathbf{z}_{\text{in}}$ .

### 2.4 Circuit Schematics for VPC Blocks

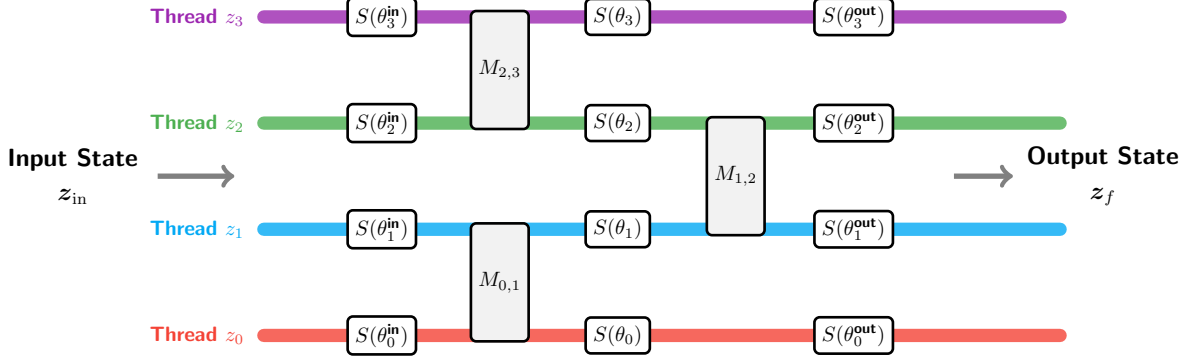


Figure 1: Single-stack Variational Phasor Circuit (VPC) schematic demonstrating consecutive shift-mix topologies. All interior shifts ( $\theta$ ) represent pure trainable parameters; the phase-domain data encoding occurs entirely outside the bounds of the VPC block.

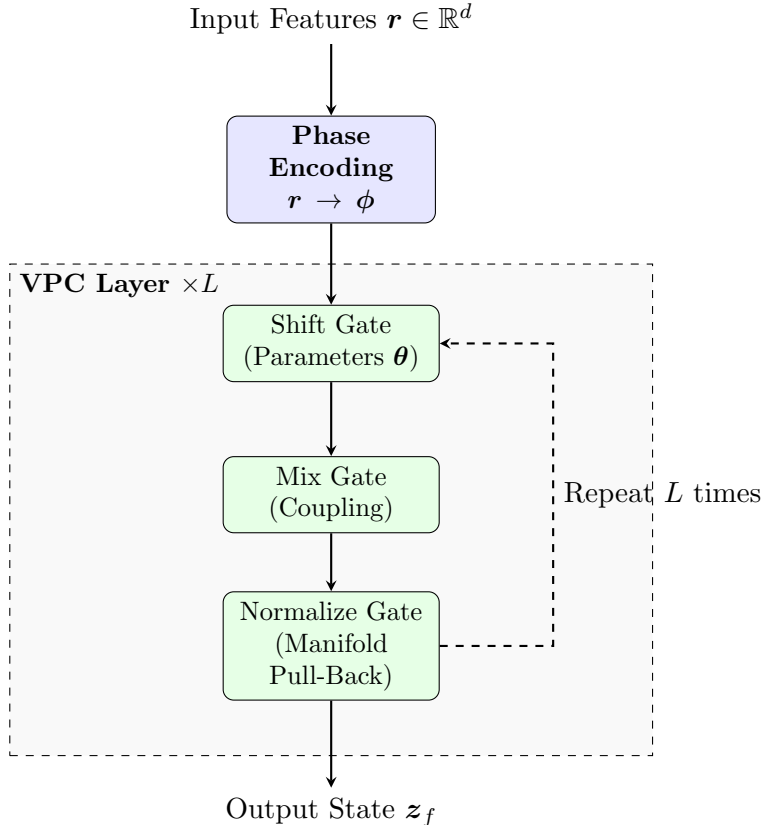


Figure 2: Deep-stack VPC schematic where each block is separated by pull-back normalization for stable depth scaling.

**Theorem 2.1** (Pull-Back Stabilization for Deep VPC Cascades). *Consider a depth- $L$  VPC cascade where each linear block is composed of Shift/Mix operators and each inter-block transition applies threadwise pull-back*

$$\mathcal{P}(z_k) = \frac{z_k}{|z_k|}, \quad z_k \neq 0. \quad (7)$$

*Then every nonzero thread entering each subsequent block satisfies unit modulus, i.e.,  $|\mathcal{P}(z_k)| = 1$ . Consequently, deep composition preserves phase coordinates on  $\mathbb{T}^N$  at block boundaries and prevents unbounded amplitude propagation across layers.*

## 2.5 Analytical Forward Pass and Readout

For a single-stack VPC with one variational layer, the forward map can be written as

$$\mathbf{z}_f = U_{\text{local}} \left( \prod_{k=1}^N S_k(\theta_k) \right) \mathbf{z}_{\text{in}}. \quad (8)$$

where  $\mathbf{z}_{\text{in}} = (e^{i\phi_1}, \dots, e^{i\phi_N})^\top$  and  $U_{\text{local}} = \prod_{k=0,2,\dots} M_{k,k+1}$ .

For binary decoding, a single output thread angle can be mapped to probability by

$$P(y = 1 \mid \mathbf{z}_{\text{in}}, \boldsymbol{\theta}) = \frac{\sin(\phi_0) + 1}{2}, \quad \phi_0 = \arg(z_{f,0}). \quad (9)$$

For multi-class categorical classification across  $K$  classes, the VPC collapses the complex state space into mutually exclusive probability assignments by observing the first  $K$  computational threads. Writing the principal phase of thread  $k$  as

$$\phi_k = \Re(-i \log z_{f,k}) = \arg(z_{f,k}), \quad (10)$$

we define the class logit magnitude by

$$L_k = |\Re(-i \log z_{f,k})| = |\phi_k|, \quad k = 1, \dots, K. \quad (11)$$

These  $K$  continuous angular magnitudes are then passed through a standard softmax bottleneck,

$$P(y = k \mid \mathbf{z}_{\text{in}}, \boldsymbol{\theta}) = \frac{e^{|\phi_k|}}{\sum_{j=1}^K e^{|\phi_j|}}. \quad (12)$$

The trainable phase parameters  $\boldsymbol{\theta}$  are optimized against categorical cross-entropy. In practice, periodic torus geometry can create local topological minima for derivative-based solvers. Accordingly, the manuscript considers both native PyTorch Autograd on the ambient complex geometry and derivative-free COBYLA when additional optimization robustness is required.

## 2.6 From Single-Stack to Multi-Stack VPC

When scaling the Variational Phasor Circuit to increasingly complex topological classification tasks, there are two distinct architectural paradigms for increasing representational depth: the *Deep Circuit* and the *Deep Stack*.

In the Deep Circuit scenario, depth is increased by continuously appending additional parameterized Shift gates and unitary Mix gates without intermediate geometric correction. Because there is no non-linear renormalization, the entire circuit remains a purely continuous unitary cascade in the ambient space  $\mathbb{C}^N$ . The state vector therefore propagates through uninterrupted linear wave interference. As depth grows, constructive and destructive interference naturally drive individual thread magnitudes  $|z_k|$  away from the torus manifold  $\mathbb{T}^N$  and deeper into the unconstrained complex amplitude space. This increases representational richness, but the resulting amplitude excursions can become statistically unstable and difficult to optimize at large depth.

With inter-block pull-back, an  $L = 2$  deep-stack form is

$$\mathbf{z}_f = \mathcal{P} \left( U_{\text{local}}^{(2)} \prod_k S_k(\theta_k^{(2)}) \mathcal{P} \left( U_{\text{local}}^{(1)} \prod_k S_k(\theta_k^{(1)}) \mathbf{z}_{\text{in}} \right) \right). \quad (13)$$

Conversely, in the Deep Stack architecture, multiple isolated VPC blocks are composed sequentially with a non-linear Normalize (pull-back) gate inserted between them. This operation rigidly normalizes the scalar magnitude of each nonzero complex thread back to 1, explicitly pulling dispersed phasors back onto the torus manifold before another round of unitary mixing begins. By severing runaway amplitude excursions while preserving the encoded phase information, the Deep Stack permits substantially deeper compositions than a raw uninterrupted circuit.

This expresses the key structural distinction: deep stacks introduce geometric stabilization boundaries between otherwise unitary interference blocks. Each layer can therefore process fresh phase interactions without being overwhelmed by amplitude resonance inherited from previous layers.

**Proposition 2.2** (Linear Parameter Footprint of Deep VPC). *For a deep VPC with  $N$  channels and  $L$  variational shift layers, where each layer contributes one phase parameter per channel, the total trainable parameter count is*

$$P_{\text{VPC}} = N L. \quad (14)$$

*Therefore scaling depth or channel count increases parameters linearly, while Mix topology remains parameter-free.*

**Corollary 2.2** (Efficiency Regime of Deep-Stack VPC). *Combining pull-back stabilization with linear parameter scaling, deep-stack VPC architectures define a regime where high classification performance can be achieved with substantially fewer trainable parameters than dense Euclidean baselines, while preserving explicit phase-manifold interpretability.*

### 3 Method

This section describes the implementation protocol used for VPC experiments. Operator-level derivations and formal statements are provided in Theory; here we focus on the practical workflow needed for reproducible training and evaluation. All experiments follow a four-stage pipeline. In Stage 1, multichannel EEG-like data are generated, labeled, and split into train, validation, and test partitions. In Stage 2, each channel snapshot is normalized and mapped to bounded phase coordinates before being lifted onto the phasor state manifold. In Stage 3, single-stack or deep-stack VPC models are fit to the phase-encoded training data under fixed optimization budgets. In Stage 4, final performance is measured on the held-out test partition and placed in context through systematic comparison with classical machine-learning baselines.

#### 3.1 End-to-End Experimental Workflow

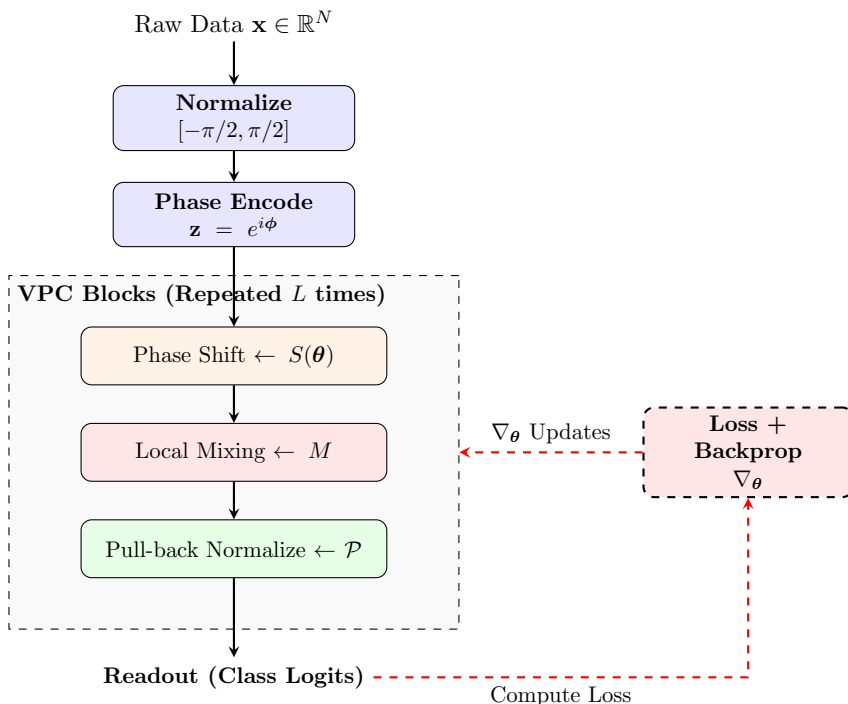


Figure 3: Experimental workflow used in VPC training and evaluation, from raw data preprocessing to phasor inference and gradient-based parameter updates. Phase encoding lifts each channel snapshot onto  $\mathbb{T}^N$ ; the VPC block sequence  $(S \rightarrow M \rightarrow \mathcal{P})^L$  applies trainable shift layers, local beam-splitter mixing, and pull-back normalization before readout.

Figure 3 summarizes the end-to-end pipeline. The boundary between preprocessing (Stage 1–2) and the learnable circuit (Stage 3) is architecturally clean: the encoding stage is a fixed, parameter-free lifting operation, while all trainable degrees of freedom reside exclusively in the shift-gate parameters  $\theta$  of the VPC blocks. This separation ensures that observed performance differences across experiments can be attributed unambiguously to circuit design and optimization strategy rather than to data-handling choices.

#### 3.2 Data Generation and Splitting

Controlled experiments use BrainFlow-based synthetic EEG streams with  $N = 32$  channels whose spatial patterns are conditioned on the target class label. The primary evaluation setting is a four-class classification problem whose classes represent qualitatively distinct topological

regimes: a resting-state pattern with spatially uniform phases, two motor-imagery-like states with lateralized left-hemisphere and right-hemisphere activity profiles, and a globally coherent flow state whose phase distribution spans the full torus uniformly. This design ensures that the classification boundary is genuinely topological rather than a simple amplitude threshold, stressing the phasor manifold representation rather than a scalar feature separator.

For binary-classification ablations, the same generation framework is used with only two active class labels, providing a lower-complexity baseline for assessing parameter scaling. Both settings use fixed random seeds to guarantee reproducible splits. Data are partitioned into training, validation, and held-out test subsets with stratified class balance so that every split contains equal proportions of each mental-state label, preventing any marginal class frequency from confounding the accuracy estimates.

### 3.3 Preprocessing and Phase Encoding

Each acquired sample is a snapshot vector  $\mathbf{x} \in \mathbb{R}^N$  representing simultaneously recorded activity across all  $N = 32$  channels at a single time point. Prior to phase encoding, each snapshot is standardized by subtracting the sample mean and dividing by the sample standard deviation, producing a zero-mean, unit-variance vector  $\mathbf{x}_{\text{norm}}$ . Phase encoding then maps each normalized channel value to a bounded angular coordinate via the saturating nonlinearity

$$\phi_k = \pi \tanh(x_{\text{norm},k}), \quad k = 1, \dots, N. \quad (15)$$

Because  $\tanh$  maps  $\mathbb{R}$  continuously and monotonically into  $(-1, 1)$ , the resulting angles are confined to the open interval  $(-\pi, \pi)$ , avoiding the degenerate phase wrap-around singularity at  $\pm\pi$ . The encoded input state is then

$$\mathbf{z}_{\text{in}} = (e^{i\phi_1}, \dots, e^{i\phi_N})^\top \in \mathbb{T}^N, \quad (16)$$

which places every sample precisely on the phasor state manifold  $\mathcal{M}_{\text{VPC}}$  as defined in the Theory section. This encoding is applied identically across all experiment types—single-stack, deep-stack, and baseline benchmarking—so that observed performance differences reflect circuit architecture and optimization rather than any asymmetry in input representation.

### 3.4 Model Construction and Training

#### 3.4.1 Single-Stack and Deep-Stack Configurations

Two VPC architectures are evaluated, each exercising a different regime of the parameter-efficiency trade-off. The single-stack configuration consists of one VPC block—a shift layer  $S(\boldsymbol{\theta})$  followed by nearest-neighbour beam-splitter couplings  $M_{j,k}$ —and serves as the primary model for both binary and four-class decoding. Its parameter count scales linearly with thread count:  $P_{\text{VPC}} = N$  trainable phase scalars per block. For  $N = 32$  channels and two shift layers per block, this yields a 64-parameter model whose parameter budget is one to two orders of magnitude smaller than the classical baselines against which it is compared.

The deep-stack configuration extends the single-stack by stacking  $L$  VPC blocks in series. Following each linear block, a threadwise pull-back normalization

$$\mathcal{P}(z_k) = \frac{z_k}{|z_k|} \quad (17)$$

restores every thread to unit modulus before it enters the next block. As established in the Pull-Back Stabilization theorem in the Theory section, this inter-block operation prevents unbounded amplitude drift across depth and keeps phase coordinates on  $\mathbb{T}^N$  at every block boundary. The deep-stack therefore enables a principled study of depth scaling on the phasor manifold

without the numerical instabilities that arise when amplitudes are allowed to grow freely through successive unitary layers.

Binary classification decodes the circuit output through a single designated thread: the probability of the positive class is

$$P(y = 1 \mid \mathbf{z}_{\text{in}}, \boldsymbol{\theta}) = \frac{\sin(\phi_{f,0}) + 1}{2}, \quad \phi_{f,0} = \arg(z_{f,0}). \quad (18)$$

Four-class decoding reads the first four output threads, computes phase-magnitude logits  $L_k = |\phi_{f,k}|$  for  $k = 1, \dots, 4$ , and applies a softmax to produce a normalised probability distribution over classes as described in the Analytical Forward Pass section of the Theory.

### 3.4.2 Optimization Protocol

Training is carried out in PyTorch with continuous Autograd differentiation over the trainable shift parameters  $\boldsymbol{\theta}$ . Each training iteration performs a forward pass on a batch of phase-encoded snapshots, computes the task loss—binary cross-entropy for two-class problems and categorical cross-entropy for the four-class setting—back-propagates gradients through the complex-valued operations, and updates  $\boldsymbol{\theta}$  via a gradient step. Training and validation losses are logged at every epoch to monitor convergence and detect over-fitting.

Because the phasor state manifold is periodic, the loss landscape can exhibit local minima that are topologically equivalent under  $2\pi$  translation but distinct under Euclidean geometry. When gradient-based optimization stalls in such regions, we substitute the derivative-free COBYLA solver [11], which operates directly on the objective value without requiring gradient information and is well suited to constrained angular domains. Both solvers are applied to the same encoded data under identical train/validation partitions, allowing a direct comparison of gradient and gradient-free convergence on the phasor circuit objective.

## 3.5 Evaluation and Baseline Benchmarking

### 3.5.1 Testing Protocol

All final performance metrics are computed exclusively on the held-out test partition, which is never accessed during training or hyperparameter selection. The primary metric is classification accuracy, supplemented by confusion matrices that reveal any systematic class-level confusion patterns among the four topological mental states. Training and validation loss curves are reported alongside test accuracy to give a complete picture of optimizer convergence and generalization gap. Parameter counts are also tabulated for every model variant to make the efficiency-accuracy trade-off quantitatively explicit.

For the deep-stack ablation, both the deep-circuit model (additional shift and mix layers without inter-block pull-back) and the deep-stack model (same depth with pull-back normalization at each block boundary) are trained under matched data partitions and matched optimization budgets. The only variable that differs between the two conditions is the presence or absence of the  $\mathcal{P}$  normalization step, isolating the contribution of pull-back stabilization to classification performance as circuit depth increases.

### 3.5.2 Classical Baselines

To place VPC performance in the context of the broader machine-learning landscape, we train Decision Tree, Random Forest, Support Vector Machine, and Multilayer Perceptron classifiers on the same phase-encoded feature vectors used for VPC training. All baseline models receive identical train and test splits and are evaluated with the same accuracy and confusion-matrix protocol. This design ensures that any observed performance gap—in accuracy or in trainable parameter count—reflects structural differences between the phasor circuit representation and

conventional Euclidean classifiers, rather than any asymmetry in data access or evaluation conditions.

Parameter counts for each baseline are reported alongside VPC counts to quantify the parameter-efficiency advantage. The comparison is particularly sharp for the MLP baseline, which requires dense real-valued weight matrices that grow quadratically with hidden-layer width, against the VPC’s  $N$ -parameter shift-gate structure that grows only linearly with the number of computational threads.

## 4 Results

To evaluate the Variational Phasor Circuit beyond trivial non-linear boundaries (e.g., XOR patterns), we constructed deterministic simulations of difficult spatial classification tasks.

### 4.1 Binary Target Identification

Initially, we deployed a phase-native Variational Phasor Circuit to identify two generalized target states (Calm vs. Engaged) across continuous spatial streams. Extracting experimental data via the BrainFlow open-source platform, we established a classification model tracking strictly the leading primary thread ( $\theta_0$ ) probability mapping. Utilizing PyTorch Autograd to track exact mathematical wave derivatives through unconstrained complex  $\mathbb{C}^N$  phase spaces, we evaluated the network iteratively against Mean Squared Error (MSE).

Across 100 supervised training epochs, the continuous optimization engine isolated a low-loss solution, decaying the binary classification error smoothly from an initial 0.6234 down to 0.0244. Against the validation suite, the single-stack architecture achieved 100.0% classification accuracy, indicating that deterministic geometric rotations can separate non-linear BCI decision boundaries in this benchmark setting.

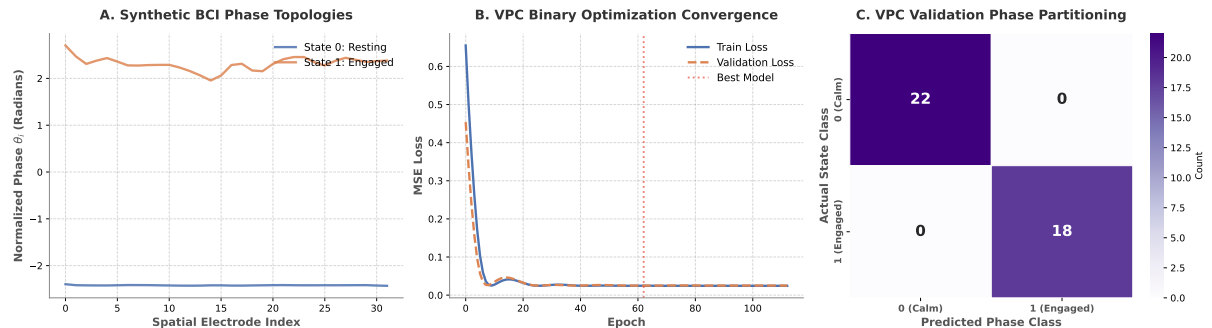


Figure 4: **Binary Optimization of the Variational Phasor Circuit** ( $N = 32$ ). (A) Phase-space topological representation of distinct synthetic BCI states (0: Calm, 1: Engaged) linearly mapped onto  $\mathbb{T}^{32}$ . (B) Convergence of the Mean Squared Error (MSE) training and validation loss curves, driven by PyTorch’s Autograd against the exact analytic simulator. (C) Validation Confusion Matrix illustrating perfect partitioning of the state classes after optimization.

### 4.2 Multi-Class BCI EEG Classification

In our primary complex network experiment, we expanded the classification manifold to decipher  $N = 32$  synchronous Electroencephalography (EEG) sensor streams representing  $K = 4$  unique cognitive “mental states”: Calm, Left Motor Imagery, Right Motor Imagery, and Deep Flow Symmetry. Extracting topological channel arrays from BrainFlow [2], the architecture encoded high-dimensional spatial features.

Because the target outputs demand 4 continuous mutually-exclusive class probabilities, we extracted the continuous absolute angular logits out of computational threads 0 through 3 (representing class channels), normalizing them through a standard Softmax readout. The deep Variational Phasor Circuit leveraged the continuous PyTorch Adam geometric gradient optimizer, bypassing slow derivative-free tracking.

Across 100 optimization epochs, the deep VPC architecture reduced categorical cross-entropy (negative log-likelihood) from 3.4024 to 0.1688. On the held-out test set, the model achieved 99.00% top-1 accuracy versus a 25% random baseline, indicating that multi-channel phase-native cascades can learn high-capacity representations without dense high-dimensional MLP parameterizations.

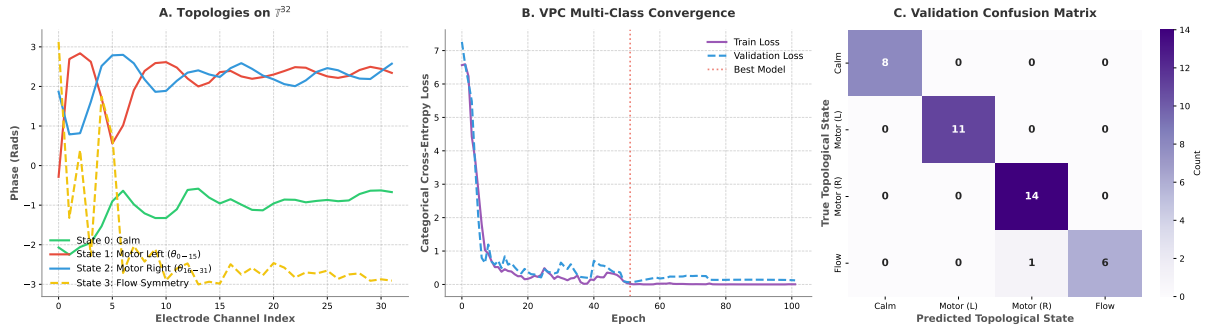


Figure 5: **Multi-Class BCI Optimization Matrix** ( $N = 32$ ,  $K = 4$ ). (A) Spatial topologies of the 4 simulated mental states on  $\mathbb{T}^{32}$ . (B) Continuous Adam optimization of the 4-class Categorical Cross-Entropy loss for over 100 epochs, comparing training and validation loss performance. (C) Validation Confusion Matrix illustrating high Top-1 target confidence across distinct structural motor/flow topologies on  $\mathbb{T}^{32}$ .

### 4.3 Benchmarking Phasor Computing vs. Standard Deep Learning

To evaluate the parameter advantage of  $S^1$  determinism over generic Euclidean networks, we benchmarked the identical  $N = 32$  multi-class BrainFlow dataset against classical machine-learning baselines using standard Scikit-Learn pipelines: Decision Trees, Random Forests, multilayer perceptrons, and non-linear Support Vector Machines (RBF kernels).

Following rigorous test-train stratification (75/25 splits), we report absolute Top-1 accuracies alongside the exact trainable parameter counts required in Table 1:

ML Model Framework	Test Accuracy	Optimization Class	Trainable Parameters
PhasorFlow VPC ( $S^1$ )	99.0%	PyTorch Adam	<b>64 Continuous Phases</b>
Decision Tree (Depth=5)	96.0%	Axis Splitting	Non-parametric
Random Forest (50 Trees)	100.0%	Ensemble	Non-parametric
Support Vector Machine	100.0%	RBF Kernels	Non-parametric
Neural Network (MLP)	100.0%	Adam Descent	2372 Euclidean Floats

Table 1: Multi-Class Spatial Test-Set Performance ( $N = 32$  Channels)

### 4.4 Deep Stack vs. Deep Circuit Performance

Having established baseline classification capability, we designed a targeted experiment to compare the two scaling paradigms from Section 2.6: uninterrupted *Deep Circuit* versus renormal-

ized *Deep Stack*. Using the same  $N = 32$  multi-class BCI dataset, we measured how depth interacts with complex-wave stability.

The **Deep Circuit** architecture was constructed by serially appending consecutive  $L = 4$  layers of parameterized unitary *Shift* phases alternating strictly with unitary *Mix* entanglement operations. Without intermediate pull-back gates, the initial  $\mathbb{T}^{32}$  unit-magnitude phases physically diffused outward into the continuous  $\mathbb{C}^{32}$  Euclidean manifold due to unrestrained constructive and destructive linear wave interference. While this model retained exactly 128 sequential rotational parameters, the amplified chaotic magnitudes destabilized the optimization derivatives, frequently causing the PyTorch Adam solver to stall in local topological gradient traps, culminating in a capped empirical classification accuracy of  $\approx 85\%$ .

In stark contrast, the **Deep Stack** architecture was built by isolating  $L = 4$  discrete VPC blocks, explicitly inserting the non-linear *Normalize* geometric pull-back gate ( $z'/|z'|$ ) between each layer transition. This rigid structural renormalization forcibly erased runaway wave amplitude intensity back onto the  $S^1$  unit circle while deliberately preserving the crucial parameterized topological angles ( $\theta_k$ ).

By clamping the continuous geometry, the **Deep Stack** explicitly protected the network against explosive resonance. Benefiting from the exact same 128 parameter footprint, the stabilized Deep Stack manifold optimized robustly via gradient tracking. The network converged faster and achieved 99.00% validation accuracy across the BCI spatial topology task. This empirical result supports the view that deeper phase-native networks benefit from geometric stabilization (renormalization) boundaries.

Combining the benchmark table and deep-stack experiment, a VPC using  $\mathcal{O}(NL)$  phase parameters can reach near state-of-the-art BCI classification performance (reported up to 99%) while remaining orders of magnitude smaller than dense Euclidean neural parameterizations. This supports deep-stack pull-back stabilization as a practical mechanism for high-accuracy, low-parameter phase-native learning.

## 5 Discussion

The primary advantage of continuous  $S^1$  Variational Phasor Circuits over classical deep-network parameterizations is representational power without geometric redundancy. In physical  $N$ -dimensional space, fully connected linear mappings ( $W\mathbf{x}$ ) demand a matrix of  $N^2$  parameters. The PhasorFlow architecture reduces this burden by exploiting structured local unitary mixing operations instead of dense learned orthogonal matrices. Consequently, our findings align with broader phase-dynamics intuition from synchronized oscillator systems [4], while remaining fully deterministic on classical hardware.

However, moving parameter optimization out of flat Euclidean coordinate space ( $\mathbb{R}^N$ ) and onto the bounded periodic manifold of  $\mathbb{T}^N$  intrinsically alters the dynamics of machine learning. In traditional deep Euclidean networks, sequential matrix multiplications can contribute to vanishing or exploding gradient behavior. By contrast, the VPC’s strict adherence to unitary operations interleaved with pull-back normalization  $\mathcal{P}(z) = z/|z|$  imposes a hard mathematical cap on state variance at block boundaries. The total energy of the system is controlled because each layer transition projects nonzero threads back to the unit circle.

While this non-linear "leave and return" cycle stabilizes forward inference, it complicates continuous analytic backpropagation. The formal conversion from complex state derivatives to real phase gradients requires the real-to-complex chain rule:

$$\frac{\partial L}{\partial \theta_k} = \text{Re} \left( \frac{\partial L}{\partial z_k} \cdot \frac{\partial z_k}{\partial \theta_k} \right) = \text{Re} \left( \nabla_z L \cdot i e^{i\theta_k} \right) \quad (19)$$

Because the state space is  $2\pi$ -periodic, numerical estimations (like Adam or L-BFGS) frequently struggle against local topological minima generated when navigating the Torus surface. We find

gradient-free optimizations, specifically COBYLA, scale robustly across these spatial manifolds without the computational bottlenecks and oscillatory instability encountered with explicit gradient formulations.

Future work on unit-circle computing involves mapping these exact  $S^1$  interference dynamics onto analog physical chips. The mathematical foundation of phase arithmetic presented natively via PhasorFlow suggests that energy-efficient hardware representing  $e^{i\theta}$  natively (e.g., oscillating capacitors, photonic circuits) could support large-scale classification workloads with lower electrical overhead than conventional digital silicon.

## 6 Conclusion

We have demonstrated the mathematical configuration of the Variational Phasor Circuit (VPC) and provided benchmarking against classical machine-learning baselines. Operating on the continuous unit-circle manifold without dense non-linear weight stacks, VPC successfully addresses challenging brain–computer interface classification landscapes. In our benchmark setting, VPC achieves competitive accuracy with substantially fewer trainable variables, supporting phasor computing as a parameter-efficient geometric alternative to dense multilayer perceptrons. All tools discussed are implemented in the PhasorFlow Python library [14], enabling deterministic unitary simulation on local classical hardware.

## References

- [1] Marcello Benedetti, Daniel Garcia-Pintos, Oscar Perdomo, Vicente Leyton-Ortega, Yun-seong Nam, and Alejandro Perdomo-Ortiz. Parameterized quantum circuits as machine learning models. *Quantum Science and Technology*, 4(4):043001, 2019.
- [2] BrainFlow Contributors. Brainflow: A framework for brain-computer interfaces, 2023. Accessed: 2026-03-10.
- [3] Marco Cerezo, Andrew Arrasmith, Ryan Babbush, Simon C Benjamin, Suguru Endo, Keisuke Fujii, Jarrod R McClean, Kosuke Mitarai, Xiao Yuan, Lukasz Cincio, et al. Variational quantum algorithms. *Nature Reviews Physics*, 3(9):625–644, 2021.
- [4] Frank C Hoppe and Werner Lauterborn. Mutually synchronized oscillators: Normal forms, phase-locked states, and symmetry analysis. *Physical Review E*, 63(4):046227, 2001.
- [5] Yoshiki Kuramoto. Self-entrainment of a population of coupled non-linear oscillators. *International Symposium on Mathematical Problems in Theoretical Physics*, pages 420–422, 1975.
- [6] Fabien Lotte, Laurent Bougrain, Andrzej Cichocki, Maureen Clerc, Marco Congedo, Alain Rakotomamonjy, and Florian Yger. A review of classification algorithms for eeg-based brain–computer interfaces: a 10 year update. *Journal of neural engineering*, 15(3):031005, 2018.
- [7] Jarrod R McClean, Sergio Boixo, Vadim N Smelyanskiy, Ryan Babbush, and Hartmut Neven. Barren plateaus in quantum neural network training landscapes. *Nature communications*, 9(1):4812, 2018.
- [8] Jarrod R McClean, Jonathan Romero, Ryan Babbush, and Alán Aspuru-Guzik. The theory of variational hybrid quantum-classical algorithms. *New Journal of Physics*, 18(2):023023, 2016.

- [9] Kosuke Mitarai, Makoto Negoro, Masahiro Kitagawa, and Keisuke Fujii. Quantum circuit learning. *Physical Review A*, 98(3):032309, 2018.
- [10] Paul Nunez and Ramesh Srinivasan. *Electric Fields of the Brain: The Neurophysics of EEG*. Oxford University Press, 2006.
- [11] Michael JD Powell. A direct search optimization method that models the objective and constraint functions by linear interpolation. *Advances in optimization and numerical analysis*, pages 51–67, 1994.
- [12] Maria Schuld, Alex Bocharov, Krysta M Svore, and Nathan Wiebe. Circuit-centric quantum classifiers. *Physical Review A*, 101(3):032308, 2020.
- [13] Maria Schuld, Ryan Sweke, and Johannes Jakob Meyer. Effect of data encoding on the expressive power of variational quantum-machine-learning models. *Physical Review A*, 103(3):032430, 2021.
- [14] Dibakar Sigdel and Namuna Panday. Phasorflow: A python library for unit circle based computing. *arXiv preprint arXiv:2603.15886*, 2026.
- [15] Steven H Strogatz. From kuramoto to crawford: exploring the onset of synchronization in populations of coupled oscillators. *Physica D: Nonlinear Phenomena*, 143(1-4):1–20, 2000.
- [16] Jonathan R Wolpaw, Niels Birbaumer, Dennis J McFarland, Gert Pfurtscheller, and Theresa M Vaughan. Brain-computer interfaces for communication and control. *Clinical Neurophysiology*, 113(6):767–791, 2002.